

Design and fabrication of a multilayered polymer microfluidic chip with nanofluidic interconnects *via* adhesive contact printing†

Bruce R. Flachsbart,^{ab} Kachuen Wong,^a Jamie M. Iannacone,^{bc} Edward N. Abante,^a Robert L. Vlach,^a Peter A. Rauchfuss,^a Paul W. Bohn,^{bc} Jonathan V. Sweedler^{bc} and Mark A. Shannon^{*ab}

Received 10th October 2005, Accepted 23rd December 2005

First published as an Advance Article on the web 17th March 2006

DOI: 10.1039/b514300d

The design and fabrication of a multilayered polymer micro-nanofluidic chip is described that consists of poly(methylmethacrylate) (PMMA) layers that contain microfluidic channels separated in the vertical direction by polycarbonate (PC) membranes that incorporate an array of nanometre diameter cylindrical pores. The materials are optically transparent to allow inspection of the fluids within the channels in the near UV and visible spectrum. The design architecture enables nanofluidic interconnections to be placed in the vertical direction between microfluidic channels. Such an architecture allows microchannel separations within the chip, as well as allowing unique operations that utilize nanocapillary interconnects: the separation of analytes based on molecular size, channel isolation, enhanced mixing, and sample concentration. Device fabrication is made possible by a transfer process of labile membranes and the development of a contact printing method for a thermally curable epoxy based adhesive. This adhesive is shown to have bond strengths that prevent leakage and delamination and channel rupture tests exceed 6 atm (0.6 MPa) under applied pressure. Channels 100 μm in width and 20 μm in depth are contact printed without the adhesive entering the microchannel. The chip is characterized in terms of resistivity measurements along the microfluidic channels, electroosmotic flow (EOF) measurements at different pH values and laser-induced-fluorescence (LIF) detection of green-fluorescent protein (GFP) plugs injected across the nanocapillary membrane and into a microfluidic channel. The results indicate that the mixed polymer micro-nanofluidic multilayer chip has electrical characteristics needed for use in microanalytical systems.

1. Introduction

Recently, a number of multiple layer microfluidic devices capable of performing electrophoretic separations and fluidic manipulations (mixing, reacting, piping, and valving) have been demonstrated.¹ To add functionality to these types of devices, a new class of hybrid microfluidic-nanofluidic devices is being developed that exploits the physical dimensions of nanoscale pores in nanocapillary membranes to allow a unique set of transport capabilities.² In particular, a number of reports detail the use of crossed microchannels made in PDMS that are vertically separated by a thin membrane containing a large array of nanocapillaries³ that permits a variety of sample manipulations, including: nanofluidic gated injection of analytes and electrophoretic separation,⁴ the mixing and

reaction of two fluid streams,⁵ the collection of a specific electrophoretically separated band,⁶ and the separation of a sample based on mass (or molecular size).⁷

The goal of this current work is to convert the PDMS construct into a polymer chip that integrates nanocapillary array membranes (NCAMs) into a multilayer structure that is scalable and can incorporate multiple analytical operations on-chip, along with the ability to move analytes sequentially through these manipulations. Moreover, the chip needs the ability to be optically interrogated using ultraviolet to visible laser induced fluorescence detection, have stable electroosmotic flow (EOF) coefficients, allow separations without excessive band spreading, and be robust with respect to electrical and mechanical properties.

The approach to designing the multilayer chip is to fabricate microfluidic channels in layers that are separated by NCAMs. Fig. 1 shows a chip with different NCAM pore sizes separating three microfluidic channel layers. Where the microchannels cross over each other, flow occurs through the NCAM when a potential difference is applied to the different microfluidic channel layers. For this demonstration, there are two sets of cross-channel interconnects at both ends of the chip for the purpose of injecting samples into and collecting samples from the long separation channel located in the center layer. The fluid and potentials are introduced to the chip through the large reservoirs along the perimeter of the chip. Fig. 2 shows

^aDepartment of Mechanical & Industrial Engineering, University of Illinois at Urbana-Champaign, Urbana, IL 61801, USA.
E-mail: mshannon@uiuc.edu; Fax: +1 217-244-6534;
Tel: +1 217-244-1545

^bBeckman Institute for Advanced Science and Technology, University of Illinois at Urbana-Champaign, Urbana, IL 61801, USA

^cDepartment of Chemistry, University of Illinois at Urbana-Champaign, Urbana, IL 61801, USA

† Electronic supplementary information (ESI) available: Photographs of a polycarbonate nanocapillary array membrane after bonding to a device stack, a PDMS temporary carrier after contact printing an adhesive layer onto a PMMA microfluidic channel layer and the setup used for pressure testing layer bond strength. See DOI: 10.1039/b514300d

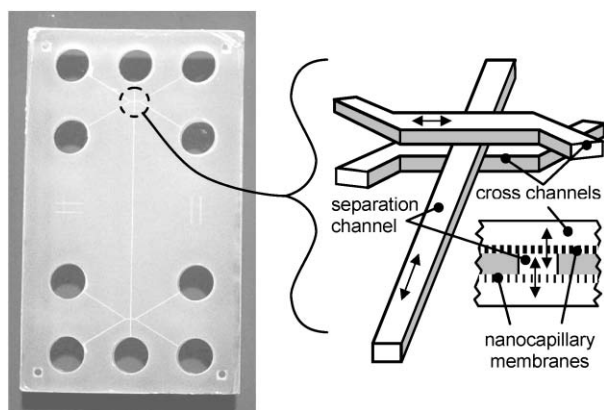


Fig. 1 A multilayer device (eight layers in total) containing three microfluidic channel layers separated vertically by two nanocapillary array membranes (NCAMs), across which fluid flows between the channels. Devices with NCAM pore diameters of 10 and 220 nm, and 10 and 100 nm have been fabricated.

explicitly the design of each layer in the chip along with its given function, and Fig. 3 shows the cross-sectional view of the microchannel at the different layers. The purpose for the different levels of cross-connect channels (levels 3 and 7) is to be able to inject buffer and sample fluids into the separation channel (level 5) from the reservoirs (level 1), and then to collect the bands in level 7 for optical spectroscopy. Level 8 is thin (5 to 10 μm) so that a high numerical aperture ($N.A. > 1$)

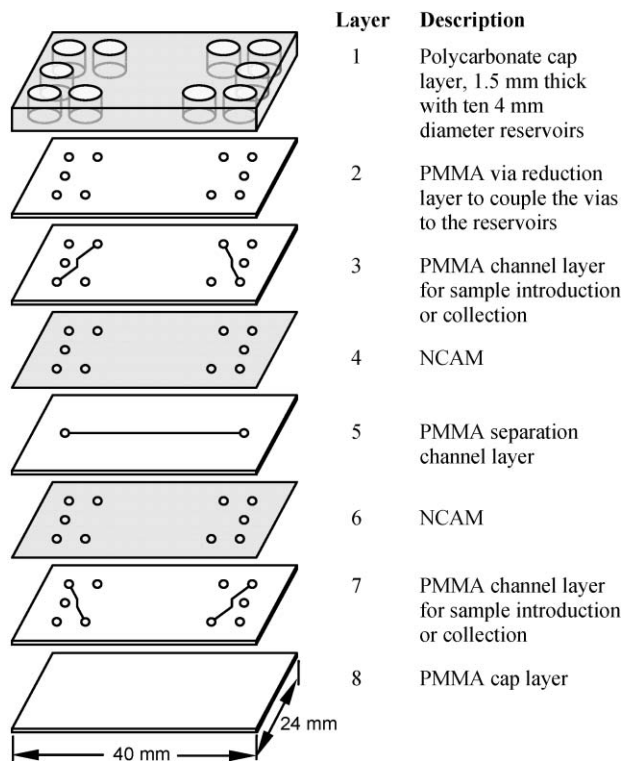


Fig. 2 Diagram depicting the individual layers in the 8-layer device shown in Fig. 1. Adhesive is contact printed onto the top and bottom surfaces of layers 3, 5, and 7. Layer 2 has adhesive contact printed only to its top surface. PMMA layers have thicknesses ranging from 5 to 40 μm . Polycarbonate NCAMs range in thickness from 6–10 μm .

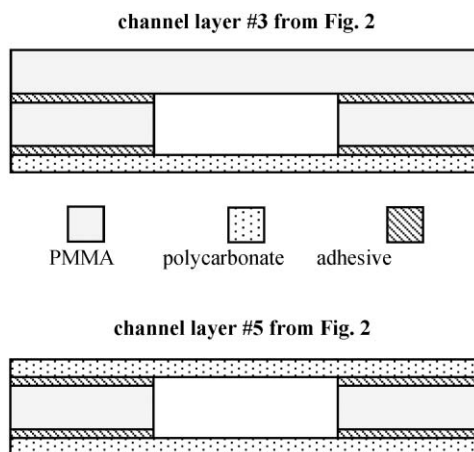


Fig. 3 Cross-sectional views of the microfluidic channels of Fig. 2 showing (a) the asymmetric nature of channel layer 3 (and similarly channel layer 7), which are bounded on three sides by PMMA and one side by a PC NCAM, as opposed to (b) the symmetric nature of channel layer 5 that is bounded on two sides by PMMA and two sides by PC NCAM. Note that a thin (<1 μm) layer of adhesive contacts the cavity in two layers for each channel layer.

microscope objective can be used to spatially resolve the products collected. By having multiple levels and channels, the process of injection and collection can occur multiple times across multiple NCAM interconnects as desired. While these demonstration chips have only two interconnect regions and three microfluidic levels, one can envision applications requiring large arrays of interconnected NCAMs across many additional levels. In order to accomplish these design goals, we need a fabrication method that is scalable to large platform areas, since microfluidic separations often span 10 to 100 mm in length. Additionally, the platform needs to be robust in mechanical strength, reproducible in form and operation, and capable of being produced in high yields.

The fabrication approach discussed here employs three relatively recent advances in polymeric microfabrication. The first advance uses a modified transfer process,⁸ where each layer is processed as if it were an independent rigid substrate, which is then transferred—aligned, bonded, and released—to the chip. The second advance uses a rigid-compliant method of transfer bonding, which is described here for the first time, and the third uses contact printing of an adhesive using elastomeric stamps. While elastomeric stamps have been used to contact print monolayer inks,⁹ thin metal films,¹⁰ and liquid polymers,¹¹ the use of contact printing in microelectromechanical (MEMS) device fabrication to pattern layers as thick as 1 μm , as in the adhesive layer printing of benzocyclobutene for wafer level bonding,¹² is relatively recent. Poly(dimethylsiloxane) (PDMS) stamps are widely used for contact printing¹³ due to their ability to conform to the surface to be printed upon, as well as their ability to be “rolled” onto that surface without trapping bubbles and particles at the interface.¹⁴ Typically the surface of the PDMS needs to be modified so that it wets and then transfers the compound being printed.

In implementing the design and approaches described here, there are many questions that must be resolved to both

fabricate and meet the operational constraints for a functioning microanalytical chip. The purpose of this paper is to: (i) describe the design, fabrication, and initial characterization of a multilayer micro–nanofluidic chip for conducting all these types of fluidic and compound manipulations; and (ii) note the major problems encountered and present the critical steps developed to solve or mitigate these obstacles in order for the device to function as desired. The following section describes the fabrication processes, including the contact printing and mechanical issues that are addressed. The initial testing of the chip is also presented, which shows that the design and fabrication method meets the set of requirements for the multilayer micro–nanofluidic chip.

2. Device fabrication

The overall fabrication scheme of the multilayer device shown in Fig. 2 consists of: (a) beginning with an essentially rigid substrate on which to build the device; (b) individually processing each distinct labile polymer layer on a separate carrier plate, including if necessary spinning and curing the polymer layer, patterning, etching, and applying the adhesive; (c) transferring, aligning, and bonding the labile polymer layer on the substrate; (d) releasing the carrier plate; and (e) repeating with subsequent layers to form a multilayer stack. After a brief overview of the assembly of the multilayer stack, sections 2.1 to 2.4 detail the major issues addressed in order to fabricate the device.

The assembly of the layers into the device in Fig. 1 consists of the sequential operations of contact printing adhesive layers, bonding, and releasing the bonded PMMA layers from their temporary coverglass carriers. An adhesive (detailed in section 2.2) is contact printed onto the top surface of PMMA layer #2 in Fig. 2, which is then bonded to the polycarbonate (PC) top piece (layer #1 in Fig. 2) at 130 °C and 5.2 MPa of applied pressure under vacuum for 10 minutes. PMMA layer #2 is processed while affixed to a temporary coverglass carrier, which, after bonding, is released by submersion in a hot water bath at approximately 50 °C for 5 min. The next PMMA layer #3 is bonded to the device stack in the same way that layer #2 is bonded, *i.e.* the top surface of PMMA layer #3 is coated with an adhesive, whereby it is bonded to the device stack, and its temporary carrier released using a hot water bath. Bonding NCAM layers requires a slightly different approach since adhesive cannot be applied directly to the NCAM layer without plugging the nanoscale pores. Thus the adhesive is to be applied to each of the layers facing the NCAM layer. Accordingly, the bottom surface of PMMA layer #3 and the top surface of the PMMA layer #5 are coated with adhesive. A NCAM layer #4 is placed between them, aligned and bonded together. After the bonding process, the coverglass carrier for PMMA layer #5 is released. The process is repeated for the second NCAM layer #6 and the PMMA layer #7. The final, unpatterned PMMA layer #8 is bonded to the device after coating the bottom of PMMA layer #7. The final step is a 12 h vacuum-oven cure at 130 °C at a temperature and time sufficient to fully crosslink all the epoxy adhesive layers without allowing the remaining solvents or curing byproducts to coalesce.

2.1 Layer processing

The first and topmost layer serves as the substrate for the chip. The substrate is a rectangular piece of PC (lateral dimensions of 24 × 40 mm, approximately 1.5 mm thick) drilled with 4 mm diameter holes that serve as the reservoirs to introduce the sample, buffer, and reagents, as well as to collect the waste. While glass and silicon can potentially be used, PC exhibits the best mechanical characteristics for multiple layer processing, as will be discussed later.

For the fabrication of the individual labile layers, two different materials are used: thin PMMA films and PC-NCAMs. The first two layers on top of the substrate, and alternating layers thereafter, are separate layers made from PMMA to form and seal the microchannels within the chip. The layers are formed by spincoating PMMA dissolved in propylene glycol monomethyl ether acetate (PGMEA) and anisole (all from Sigma Aldrich) onto a coverglass (Fisher Scientific, 35 × 50 mm, #2 thickness) that acts as the carrier plate for the PMMA layer. The PMMA on the coverglass is cured to 180 °C in an oven for 6 to 24 hours depending on layer thickness.

After curing, the PMMA layer is patterned on the carrier plate to form the required channels and vias, as seen in Fig. 1 and 2. To form the patterns, a layer of aluminium, *ca.* 100 nm thick, is sputter coated onto the PMMA and patterned using standard photolithographic procedures. The development of the positive photoresist etches the aluminium layer, thereby transferring the mask pattern to the aluminium layer. The areas of PMMA not protected by photoresist and aluminium are removed by reactive ion etching (RIE) using an oxygen and argon plasma (Axic RIE, 600 W). Fig. 4 shows an example of two PMMA channel layers after RIE processing, with a channel cross-section shown in the inset. As will be discussed in section 2.2, a straight profile created during this etch step is important for the chip's operation. The final step in the preparation of the PMMA layers is the removal of the aluminium layer with photoresist developer, which also removes any remaining photoresist residue.

The fourth and sixth layers shown in Fig. 2 are commercially available nanocapillary PC membranes (GE Osmonics Labstore). These membranes are nuclear track etched to produce nanometre scale diameter cylindrical pores through

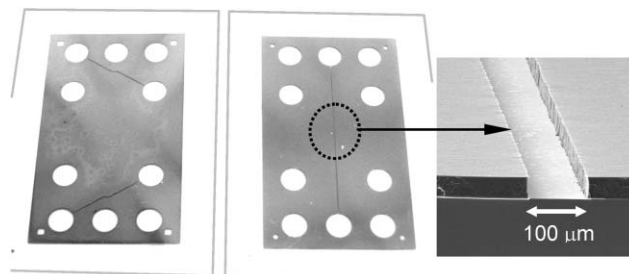


Fig. 4 Examples of PMMA channel layer #3 (left) and #5 (right) on coverglass carriers (outlined in gray), consisting of PMMA patterned by RIE using aluminium mask layers. Inset shows a close-up of the etched channel in layer #5. In the inset, the sample was cleaved in half to produce an edge view showing the straight sidewalls of the PMMA and the thin adhesive bond thickness.

the membrane. The membranes are supplied with a thin polyvinylpyrrolidone (PVP) coating to make the layers hydrophilic. Polycarbonate is naturally hydrophobic, and without the PVP coating, filling both the microfluidic channels and nanocapillaries would be difficult. The hydrophilic PVP coating, though, causes problems with delamination, as will be discussed in section 3. Membranes can be obtained with nominal pore diameters ranging from 10 nm to 400 nm and come in circular sizes of various diameter. Only 47 mm diameter membranes were used in this work. The NCAMs are temporarily mounted onto PDMS disks using methanol, so that they are lying flat when aligned and bonded to the device stack. Since the membrane (47 mm diameter) is larger than the device (24 × 40 mm) the excess overhanging membrane is trimmed after bonding the membrane to the device using a razor blade. Then vias are opened in the NCAM using oxygen etching with a Si-shadow mask. Note that the vias are 4 mm in diameter and etching resolution issues are not significant.

2.2 Contact printing of adhesive

The transfer process consists of spincoating a temporary carrier with adhesive, which is then transferred by pressing the adhesive onto the desired layer to be bonded. In order to prevent adhesive from plugging the nanopores in the NCAM, the adhesive is contact printed only onto the patterned surfaces of the PMMA layers.

The epoxy adhesive is a mixture of Dow Corning solid epoxy novalac-modified resin with curing agent in a 2.5 : 1 mass ratio, and various solvents (2-methoxyethanol 15 to 50% by mass range, anisole 15 to 50% by mass range, and PGMEA 0 to 10% by mass range, the exact amounts depend upon the adhesive layer thickness desired). Most often, the solvents are selected to modify the viscosity of the adhesive in order to achieve a thickness of 1 μm *via* spincoating and to achieve sharp interfaces.

The temporary adhesive carrier used for contact printing the adhesive layer is a 50 mm diameter PDMS disk that is 3 mm thick, created using the standard Dow Corning Sylgard 184 ratio and cure recipe. Optical microscope inspection after contact printing is used to monitor the degree to which the pattern is resolved during the contact printing procedure. The resolution is determined by the smallest dimension that can be printed without “bridging” and/or seeping of the adhesive into the channel, as shown in Fig. 5. If a printed layer has errors, the PMMA surface can be reprinted with adhesive after removing the previous layer with methanol. Features of 100 μm can be resolved using an adhesive layer approximately 1 μm thick. Thinner adhesive layers generally achieve better transfer resolution, but also tend to be harder to release from the carrier substrate and cannot accommodate local non-uniformities, which will be discussed later.

Another factor that affects contact printing resolution is the temperature of the adhesive carrier. PDMS has a greater affinity to the adhesive layer when it is cold, and the affinity decreases with increasing temperature. Heating the PDMS carrier and adhesive to 50 °C for 3 min improves the transfer of adhesive to the areas in contact with the PMMA surface. The chip and adhesive carrier are then cooled to improve the

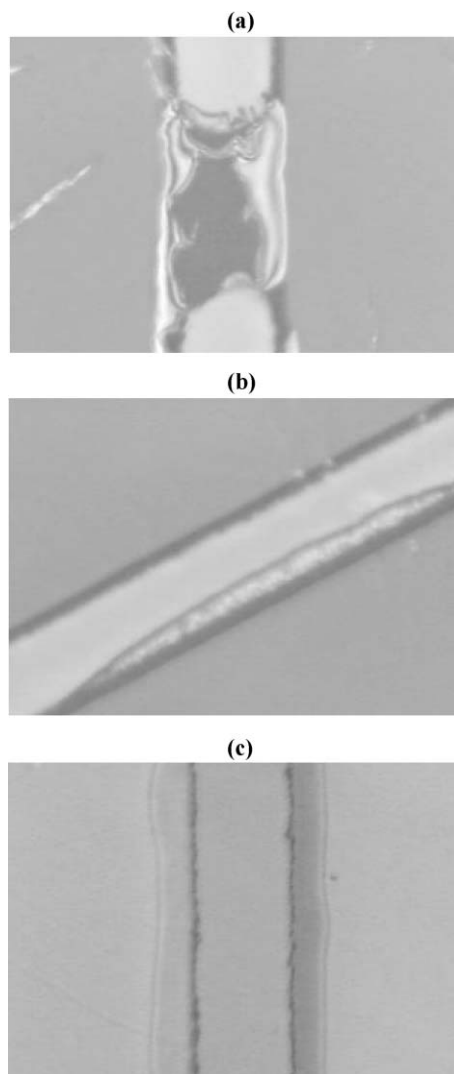


Fig. 5 Optical images from a microscope of 100 μm wide microfluidic channels after contact printing adhesive where in (a) adhesive has “bridged” the channel, (b) the adhesive has seeped into the microchannel, and (c) the adhesive prints only to the edge of the channel.

adhesion of the adhesive that is not in contact with the surface, and the PDMS carrier is removed. This heating and cooling of the adhesive carrier substantially benefits the yield of the process in addition to significantly improving the contact printing resolution.

Finally, a major issue with contact printing resolution is the sidewall profile of the PMMA channels. As will be discussed, channels with vertical sidewalls and sharp adhesive layers produce the best electroosmotic flow characteristics for these devices. Our initial PMMA patterning used oxygen–argon etching with microfabricated silicon shadow masks. This process produced trapezoidal channel side profiles as shown in Fig. 6(a) with rounded edges that together gave a roll-off of greater than 10 μm per side. Fig. 6(b) shows a typical problem with adhesive that is contact printed to the trapezoidal channel profiles of Fig. 6(a). Without a sharp edge to the channel, it is difficult to produce a sharp edge with the adhesive, leading to adhesive entering the microchannel cavity. The presence of

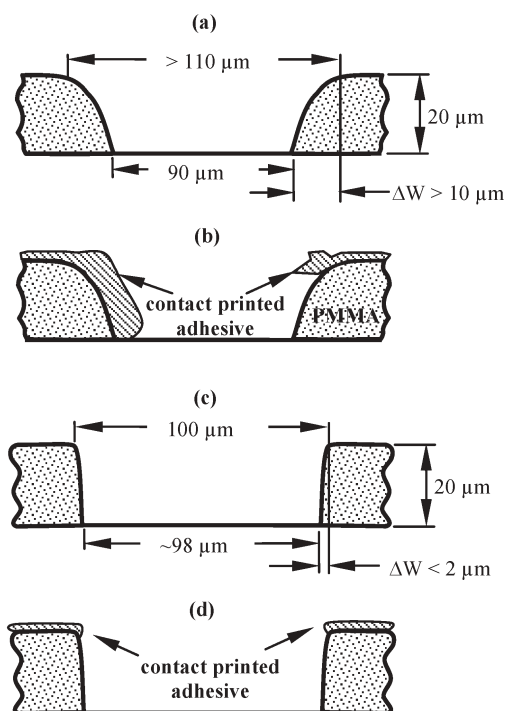


Fig. 6 Concept drawing of RIE etching with roll-off of PMMA channel layers and its effect on adhesive contact printing. The channel sidewall profiles for PMMA channel layers fabricated *via* two methods where (a) and (b) are by silicon shadow mask etching and (c) and (d) are by patterned aluminium etching. Fig. 6 (a) and (c) depict the channels before contact printing and Fig. 6 (b) and (d) depict after printing. A larger than fivefold improvement in sidewall profile aspect ratio is achieved in adhesive edge control as depicted in (d) over (b).

adhesive in the channel can bridge the channels, as shown in Fig. 5(a), blocking flow. However, even when the adhesive seeps into the channel as seen in Fig. 5(b) and the left hand side of Fig. 6(b), or gathers at the corner as depicted in the right hand side of Fig. 6(b), the presence of the adhesive tends to interfere with electroosmotic flow (EOF). For the same reasons, others have also found that preventing adhesive from entering the microchannels is of “utmost importance.”¹⁵ Changing fabrication techniques to patterned aluminium layers brings the RIE mask, which is three orders of magnitude thinner than the earlier silicon shadow masks, into intimate contact with the PMMA surface. Fig. 6(c) depicts the reduction in roll-off to less than 2 μm per side, providing a fivefold increase in channel side wall profile aspect ratio, which enables a defined edge to the contact printed adhesive layer, as depicted in Fig. 6(d). With uniform, thin (less than 1 μm) adhesive layers, the electroosmotic flow through microchannels of either type shown in Fig. 3 is reproducible, as is discussed in section 3.

2.3 Planarity

Another important issue is maintaining planarity as each layer is added to the stack. Variations in the rigid substrate and carrier plates due to size control, warpage, and curvature, result in global non-uniformity on the order of tens of microns over millimetres in the bonding of layers, with some local

vertical variations in the range of microns over 100 μm horizontal distance. Note that curvature of the layered substrate can result from variations in the initial lot *and* subsequent processing steps that induce residual stresses. In addition, variations in the thickness of each labile PMMA and nanoporous PC layer lead to local non-uniformities on the order of nanometres to microns of horizontal distance, and microns of global non-uniformities. With the addition of each layer, the global non-uniformities tend to be additive, making sequential bonding of layers more difficult.

To mitigate the additive effects of the variations in size and shape, global and local non-uniformities must be addressed separately. The local non-uniformities proved easier to mitigate by requiring each labile layer to fully cover each layer across the chip. A convenient chip size of 24 × 40 mm is chosen because it fits inside the standard membrane size of 47 mm, and it approximates the usable dimension of the PMMA coated coverglass (35 × 50 mm) after the areas affected by the edge bead are removed (generally 2 to 5 mm per side). Elimination of step-height differences by requiring full layer coverage, and the elimination of individual layer thickness variations greater than 1 μm, enabled the fabrication of the 8 layer chips shown in Fig. 1. Secondly, local sub-μm non-uniformities can be accommodated by the adhesive layer being approximately 1 μm thick. Finally, the global non-uniformity issue is mitigated by using a rigid-compliant assembly step discussed in section 2.4.

2.4 Mechanical material constraints

There are three primary mechanical issues encountered in the fabrication of the chip: (1) global non-uniformities (surface warpage and curvature) caused by initial variations and residual stresses induced during fabrication and layering; (2) rigidity of the substrate and carrier plates that do not allow local non-uniformities (defects or sub-μm debris between the layers) to be accommodated; and (3) coefficient-of-thermal-expansion (CTE) induced stresses (the chip temperature during fabrication varies between 10 and 130 °C) that enhance delamination. Excessive bonding pressure applied to force the layers to span both global and local non-uniformities results in the fracture of the substrates and/or tearing and deformation of the NCAMs or PMMA layers. For these reasons a new method described below accommodates all the variations in the multiple layers.

When bonding multilayered structures, the compliance between the individual layers and their carrier substrates determines the overall quality of the bonds between layers. One advantage for using PDMS carrier substrates is that the large compliance of a relatively thick (>100 μm) PDMS elastomer layer can accommodate many microns of non-uniform layers. However, the much higher (2 to 3 orders of magnitude) modulus of PMMA and PC materials make these layers much more rigid. So the selection of the carrier plates for transferring layers to the substrate is important. For global non-uniformities, the carrier for the PMMA layers is a 0.2 mm thick coverglass because it can bend to match the surface it is being bonded to. During bonding, an elastomeric polymer is used to apply uniform pressure to the back of the coverglass

carrier so that the PMMA globally conforms to the chip surface onto which it is being bonded. The NCAM is bonded using a temporary PDMS carrier so that the membrane can conform to the multilayer stack.

The CTE mismatch induces stresses in the PMMA and PC layers that can delaminate the layers, either spontaneously or at low applied fluid pressures within the channels. The CTE mismatch is approximately an order of magnitude larger between PMMA and glass or silicon. Attempts to bond PMMA or PC layers to these substrates resulted in shattered glass, cleaved silicon, or ripped polymer layers. A PC reservoir top piece resulted in an all-polymer chip and reduced the CTE induced stresses enough that chips can be fabricated using contact printable thermally cured adhesive and can sustain applied fluid pressures above 6 atm. Using these methods to maintain planarity has thus far allowed more than 11 PMMA/NCAM layers to be stacked and bonded.

3. Chip testing and discussion

The pressure that the chip can sustain without failure by rupture or delamination is one important indicator of robustness of the fabrication process and chip operation. The use of PVP-coated nanoporous PC membranes to serve as the NCAM leads to problems with side channel leakage and subsequent delamination due to hydrophilic capillary forces. The wetting angle, θ , on PVP-coated PC is *ca.* 45° or smaller. Thus, if water wicks into the small radii pores (10 to 220 nm), the capillary head pressure pulling in the water can be quite high, providing a driving force for seepage of water between the layers, especially if the pores are not fully sealed by the adhesive. Although it is difficult to calculate and/or measure the additional capillary pressure of water at the PMMA/NCAM interface, a simple estimate is $P_{\text{eff}} = \pi\gamma_{\text{lv}}\cos(\theta)/2\alpha^2r$, where γ_{lv} is the liquid–vapor surface tension of water (0.0728 N m⁻¹ at 25 °C), α is the average pore spacing to diameter ratio, and r is the radius of the pore. P_{eff} essentially adds a hydrostatic fluid pressure between the layers that ranges for $\alpha = 4$ (which is approximately the case for the membranes used here) from a low of ~0.5 atm for 220 nm pores to nearly 10 atm for 10 nm pores. We observed that when the adhesive did not fully seal the pores, the wetting led to delamination at very low applied fluid pressures, particularly for the smallest pore sizes. If glass or silicon is used instead of PC for the substrate, the higher CTE mismatch creates additional stresses, so that simply adding water to the channels, without any applied pressure, can cause spontaneous delamination. By adjusting the viscosity and printing of the adhesive, the adhesive completely seals the pores at the edges to prevent leakage and to sustain high pressures without delamination.

The chip layer bond strength is pressure tested by fabricating modified chips whose reservoirs are tapped to accommodate high pressure hose fittings (Legris). After filling a channel with fluorescent solution, both ends of the channel are pressurized with nitrogen. The channel is monitored under a microscope during the pressurization process to detect delamination of the layers. Nitrogen pressure is slowly increased until chip failure occurred. The only failure mechanism observed is the rupture of the reservoir bottom

and not channel rupture or delamination between the PMMA and NCAM layers. Reservoir rupture typically occurred above 6 atm (0.6 MPa). If these chips are to be used in HPLC systems where more than 6 atm pressure is required, the reservoir can be redesigned to prevent rupture.

While wetting of the adhesive and sealing of the pores is essential for preventing delamination, seeping and bridging as shown in Fig. 5 can occur and the corners of the channels can become filled if the adhesive overwets the PMMA. This problem can also lead to blockage of nanopores at the junctions, as well as the microchannels. Seepage of adhesive, combined with rolled-off edges due to poor RIE etching as seen in Fig. 6, also causes variability in the electroosmotic flow within channels and between different chips. Therefore, achieving the right balance of adhesive wetting and edge resolution is also important for the chip's electrical operation.

The fluidic electrical resistance is measured for two regions within the chip: the long separation channel and the shorter cross channels. Such measurements verify the integrity of the microfluidic elements and uncover issues with the adhesives or the processing affecting the NCAMs lining the channels. Electrical characterization is performed on chips containing only a single membrane (220 nm) to avoid convolving effects from multiple membranes on the measurements. The resistance per unit length, R' , of the solution across the two regions is measured by monitoring the current, i , within the microchannel environments at a series of voltage differences, ΔV . The resistance is calculated as an average value from $R' = (\Delta V / \Delta l) / i$, where Δl is the length of the region. The channels are filled under vacuum with an electrolyte solution of 10 mM phosphate buffer (PB) in DI water at a pH of 7.4, with a measured conductivity of $1.124 \times 10^{-3} (\Omega \text{ cm})^{-1}$ using Thermo Orion Conductivity Meter model 105Aplus. Platinum electrodes (Goodfellow) are inserted into the corresponding solution reservoirs, and a voltage difference is applied across each microchannel. Linear I - V plots ($R^2 > 0.995$) are obtained, and the resistances of the spatially separated microchannels are calculated. A mean of $26.7 \pm 0.4 \text{ M}\Omega \text{ cm}^{-1}$ is obtained for the longer microfluidic channel ($\Delta l = 2.80 \text{ cm}$), and $37.6 \pm 0.2 \text{ M}\Omega \text{ cm}^{-1}$ for the shorter cross channels ($\Delta l = 1.23 \text{ cm}$). Although R' is an extensive property of the chip and solution, the measured values are comparable to those expected for the 10 mM PB solution with the conductivity previously given and an average of the electroosmotic flow mobilities given in Table 1 ($2.8 \times 10^{-4} \text{ cm}^2 \text{ V}^{-1} \text{ s}^{-1}$). For the 100 μm wide by 20 μm high channels, the expected resistance per unit length is $34.6 \text{ M}\Omega \text{ cm}^{-1}$, which is near the average for all the channels of $32.1 \pm 0.5 \text{ M}\Omega \text{ cm}^{-1}$. No measurable leakage current is observed through the chip itself, indicating no discernable fluid leaks between levels

Table 1 Electroosmotic coefficients ($\text{cm}^2 \text{ V}^{-1} \text{ s}^{-1}$) for phosphate buffer solution *versus* pH measured using the current monitoring method

	Long channel	Average of two cross channels
pH 4.4	$2.2 \pm 0.3 \times 10^{-4}$	$2.5 \pm 0.9 \times 10^{-4}$
pH 7.3	$3.5 \pm 0.7 \times 10^{-4}$	$2.8 \pm 0.5 \times 10^{-4}$
pH 8.8	$3.3 \pm 0.6 \times 10^{-4}$	$2.7 \pm 0.6 \times 10^{-4}$

and the inherent electrical insulating property of PMMA and PC.

Next, the electroosmotic flow (EOF) characteristics are reported. The EOF coefficients given in Table 1 are measured for the same two regions within the chip using the current monitoring method previously described.¹⁶ Briefly, the chip is filled under vacuum with 10 mM PB in DI water and conditioned for approximately 5 minutes with the application of 50 V across the different regions. Then, for each of the regions tested, one reservoir is loaded with 5 mM PB before applying 100 V across the corresponding microchannel. The change in current with respect to time is monitored as the 5 mM solution replaces the 10 mM, and a current plateau is reached. The average electroosmotic mobilities reported in Table 1 are calculated from three measurements on the same chip. These EOF values are within a factor of two of other published EOF values for all PMMA channels, which are noted to vary with processing techniques as well.¹⁷ In Kirby and Hasselbrink's review of microfluidic substrates "PMMA shows perhaps the most disagreement between investigators of all the polymers reviewed here. No clear agreement appears from the data regarding either pH dependence, concentration dependence, or relative magnitude of the zeta potential."¹⁸

It is important to note, however, that the microchannels of this multilayer chip with alternating PMMA and NCAM layers, are not made entirely of the same material. Referring to Fig. 3, the cross channels at layers 3 and 7 have PMMA on three sides for a total of 140 μm wetted perimeter, and 100 μm wetted perimeter for the PC NCAM. Conversely, the long separation channel has 40 μm and 200 μm wetted perimeters for the PMMA and PC NCAMs, respectively. If the walls had large differences in EOF mobility, we would expect to see even larger differences in the average EOF coefficients measured, since the difference in wetted perimeters between the two cases is 350% for the PMMA and 200% for the PC NCAM. The observed differences, however, are less than 25% for all cases, which is nearly within the uncertainty for the channels. Finally, the effect on the EOF of adhesive at the corners shown in Fig. 6(b) vs. 6(d) appears to be at most 36% given by the uncertainty. As noted earlier, channels with significant corner beads of adhesive experienced significantly larger variability between chips (much greater than 100%).

In order to demonstrate the transport of fluid across the NCAM and between the spatially separated microchannels, experiments are performed using laser-induced fluorescence detection. The chip is filled under vacuum with the same 10 mM phosphate buffer solution, while only one of the shorter cross channels contained an addition of 1 μM of green-fluorescent protein (GFP). A 488 nm Ar^+ laser is focused by a 10 \times objective to a spot in the longer, receiving channel immediately following the NCAM interconnect. An electric bias is applied to facilitate transport from the GFP-containing channel, through the NCAM, and into the receiving channel that does not contain the analyte. The resulting fluorescence intensity is collected with a photomultiplier tube (Hamamatsu) as part of the LIF experimental setup. Fig. 7 shows a series of transported GFP plugs through the NCAM in a phosphate buffer solution. The plug injections are confined and reproducible, represented by the symmetrical peaks and the

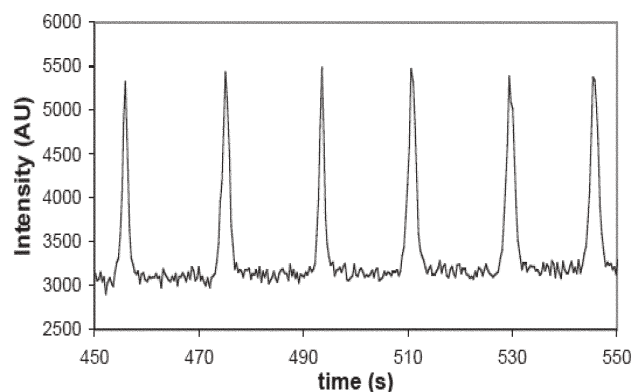


Fig. 7 Laser-induced fluorescence (LIF) detection of 1 μM GFP in 10 mM PB injected for 2 s at 600 V from one microfluidic channel, across a NCAM, and into a second microfluidic channel containing the PB solution only. Analyte peaks are reproducible and have a symmetrical shape within 9.6% RSD of the integrated peak areas.

9.6% RSD of the integrated peak areas, respectively. The chips described here have the same or better efficacy for injection as the PDMS/PC NCAM devices previously reported in our laboratory.⁴

4. Conclusions

A design and fabrication scheme is detailed so that PMMA/PC NCAM based chips can be used for electrophoretic separations and other analytical manipulations. The process produces high quality devices that can incorporate as many fluidic layers as needed. These devices allow greatly improved nanofluidic to microfluidic interfacing, especially as each layer can be optimized for a particular task. The ability to stack layers and incorporate multiple nanocapillary arrays into a single device opens up a range of complex operations and architectures that can be optimized for applications ranging from sample cleanup and preparation to multistage separations and sample collection.

Acknowledgements

This work was partially supported by National Science Foundation's *The WaterCAMPWS*, a Science and Technology Center of Advanced Materials for the Purification of Water with Systems under the agreement number CTS-0120978, the Center for Nano-Chemical-Electrical-Mechanical Manufacturing Systems under DMI-032-28162, and by Strategic Environmental Research and Development Program under Army W9132T-05-2-0028.

References

- 1 R. H. Liu, M. A. Stremler, K. V. Sharp, M. G. Olsen, J. G. Santiago, R. J. Adrian, H. Aref and D. J. Beebe, *J. Microelectromech. Syst.*, 2000, **9**, 190; B. L. Grey, D. Jaeggi, N. J. Mourlas, B. P. Driehuisen, K. R. Williams, N. I. Maluf and G. T. A. Kovacs, *Sens. Actuators, A*, 1999, **77**, 57; S. M. Kugelmass, C. Lin and S. H. DeWitt, *Proc. SPIE-Int. Soc. Opt. Eng.*, 1999, **3877**, 88; B. H. Jo, L. M. Van Lerberghe, K. M. Motsegood and D. J. Beebe, *J. Microelectromech. Syst.*, 2000, **9**, 76; J. R. Anderson, D. T. Chiu, R. J. Jackman, O. Cherniavskaya, J. C. McDonald,

- H. Wu, S. H. Whitesides and G. M. Whitesides, *Anal. Chem.*, 2000, **72**, 3158; B. H. Weigl, R. Bardell, T. Schulte, R. Battrell and J. Hayenga, *Biomed. Microdevices*, 2001, **3**, 267; J. C. McDonald, M. L. Chabiny, S. J. Metallo, J. R. Anderson, A. D. Stroock and G. M. Whitesides, *Anal. Chem.*, 2002, **74**, 1537; T. Thorsen, S. J. Maerkl and S. R. Quake, *Science*, 2002, **298**, 5593, 580; M. Agirregabiria, F. J. Blanco, J. Berganzo, M. T. Arroyo, A. Fullaondo, K. Mayora and J. M. Ruano-Lopez, *Lab Chip*, 2005, **5**, 545; D. Mijatovic, J. C. T. Eijkel and A. van den Berg, *Lab Chip*, 2005, **5**, 492.
- 2 A. N. Chatterjee, D. M. Cannon, Jr., E. N. Gatimu, J. V. Sweedler, N. R. Aluru and P. W. Bohn, *J. Nanopart. Res.*, 2005, **7**, 507–516; A. Yaroshchuk, O. Zhukova, M. Ulbricht and V. Ribitsch, *Langmuir*, 2005, **21**, 6872; A. Plecis, R. B. Schoh and P. Renaud, *Nano Lett.*, 2005, **5**, 1147; R. Karnik, R. Fan, M. Yue, D. Li, P. Yang and A. Majumdar, *Nano Lett.*, 2005, **5**, 943; T. C. Kuo, L. A. Sloan, J. V. Sweedler and P. W. Bohn, *Langmuir*, 2001, **17**, 6298.
- 3 T. C. Kuo, D. M. Cannon, Jr., M. A. Shannon, P. W. Bohn and J. V. Sweedler, *Sens. Actuators, A*, 2003, **102**, 223.
- 4 D. M. Cannon, Jr., T. C. Kuo, P. W. Bohn and J. V. Sweedler, *Anal. Chem.*, 2003, **75**, 2224.
- 5 T. C. Kuo, H. K. Kim, D. M. Cannon, Jr., M. A. Shannon, J. V. Sweedler and P. W. Bohn, *Angew. Chem., Int. Ed.*, 2004, **43**, 1862.
- 6 J. J. Tulock, M. A. Shannon, P. W. Bohn and J. V. Sweedler, *Anal. Chem.*, 2004, **76**, 6419.
- 7 T. C. Kuo, D. M. Cannon, Jr., Y. Chen, J. J. Tulock, M. A. Shannon, J. V. Sweedler and P. W. Bohn, *Anal. Chem.*, 2003, **75**, 1861.
- 8 J. C. Selby, M. A. Shannon, K. Xu and J. Economy, *J. Micromech. Microeng.*, 2001, **11**, 6, 672.
- 9 L. H. Dubois and R. G. Nuzzo, *Annu. Rev. Phys. Chem.*, 1992, **43**, 437; A. Kumar and G. M. Whitesides, *Appl. Phys. Lett.*, 1993, **63**, 2002.
- 10 Y. L. Loo, R. L. Willett, K. W. Baldwin and J. A. Rogers, *Appl. Phys. Lett.*, 2002, **81**, 562; H. Schmid, H. Wolf, H. Riel, S. Karg, B. Michel and E. Delamarche, *Adv. Funct. Mater.*, 2003, **13**, 145.
- 11 M. Wang, H. G. Braun, T. Kratzmüller and E. Meyer, *Adv. Mater.*, 2001, **13**, 1312.
- 12 J. Oberhammer and G. Stemme, *J. Microelectromech. Syst.*, 2005, **14**, 419.
- 13 P. Thiebaud, L. Lauer, W. Knoll and A. Offenhausser, *Biosens. Bioelectron.*, 2002, **17**, 87; E. Delamarche, C. Donzel, F. S. Kamounah, H. Wolf, M. Geissler, R. Stutz, P. Schmidt-Winkel, B. Michel, H. J. Mathieu and K. Schaumburg, *Langmuir*, 2003, **19**, 8749; K. M. Choi and J. A. Rogers, *Mater. Res. Soc. Symp. Proc.*, 2003, **788**, 491; K. M. Choi and J. A. Rogers, *Mater. Res. Soc. Symp. Proc. (Nanoengineered Assemblies and Advanced Micro-Nanosystems)*, 2004, **820**, 147; H. H. Lee, E. Menard, N. G. Tassi, J. A. Rogers and G. B. Blanchet, *Mater. Res. Soc. Symp. Proc.*, 2004, **846**, 159; T. E. Balmer, H. Schmid, R. Stutz, E. Delamarche, B. Michel, N. D. Spencer and H. Wolf, *Langmuir*, 2005, **21**, 622.
- 14 Y. Xia and G. M. Whitesides, *Angew. Chem., Int. Ed.*, 1998, **37**, 550.
- 15 Z. Huang, J. C. Sanders, C. Dunsmor, H. Ahmadzadeh and J. P. Landers, *Electrophoresis*, 2001, **22**, 3924.
- 16 X. Huang, M. J. Gordon and R. N. Zare, *Anal. Chem.*, 1988, **60**, 1837.
- 17 Z. Chen, Y. Gao, R. Su, C. Li and J. Lin, *Electrophoresis*, 2003, **24**, 3246.
- 18 B. J. Kirby and E. F. Hasselbrink, Jr., *Electrophoresis*, 2004, **25**, 203.